Research on heating and defrosting performance of air source heat pump system based on composite phase change materials

Yangchi Wu, Zhongbao Liu, Xuebin Jiang, Yutao Huo, Zhipeng Qie*, Zhong Wang

1. College of Mechanical and Energy Engineering, Beijing University of Technology, Beijing, 100124, China
2. China National Accreditation Service for Conformity Assessment (CNAS), Beijing, 100062, China
Corresponding authors: qiezhipeng@bjut.edu.cn (Z.Q.)

The performance of air source heat pump systems is limited in extreme climate conditions, especially in heating mode, which may face defrosting problems, resulting in energy waste and reduced system efficiency. In order to improve this problem, this article uses 5% expanded graphite/paraffin composite phase change material to preheat the heat accumulator while heating the room, and evaluates the heating and defrosting performance of the air source heat pump based on composite phase change materials. Experimental results show that after using the regenerator, the defrost evaporation period in the defrost cycle is reduced by 42.2%, the resume heating period is reduced by 38.7%, the compressor power consumption is reduced by 42.1% compared with the original system, and the average outlet temperature of indoor unit increased by 8.1 ° C, and the indoor temperature fluctuation is reduced. This research is of great significance to the performance optimization of air source heat pumps under frost-prone conditions.

Key words: Air-source Heat Pump, Phase Change Material, Defrosting, Heat Storage Technology, Enhanced Heating Performance

1. Introduction

Air-source heat pumps, which use the virtually limitless air as a heat source and sink, have attracted widespread attention[1,2]. However, the frost formation that occurs under low-temperature, high-humidity conditions significantly limits the performance of air-source heat pumps[3,4]. In winter, when the outdoor air temperature falls below the dew point and relative humidity is high, the frosting on the evaporator of the air-source heat pump intensifies[5]. Commercial air source heat pumps typically operate down to outside temperatures of approximately -25 degrees Celsius. Within this operational range, frost formation not only increases thermal resistance but also increases airside resistance. This significantly reduces heat exchange efficiency, decreases overall system performance, and can even lead to system shutdown.[6–9] .

In the optimization of air-source heat pump systems, exploring anti-frost measures is of great significance. Some researchers have started by modifying the air parameters at the outdoor coil inlet, such as relative humidity and air temperature. Su et al. [10] proposed a new frost-free air-source heat pump that combines liquid desiccant dehumidification and compression-assisted regeneration, and introduced a novel compression-assisted regeneration method to recover the regeneration heat. Under the same operating conditions, the COP of the mixed frost-free system is at least 36.05-61.19% higher than that of a traditional reverse-cycle defrosting heat pump. Other scholars have focused on improving the outdoor air inlet temperature to enhance air-source heat pump performance. Kwak et al. [11] added electric heating equipment at the outdoor unit's air inlet to raise the temperature of the air entering the unit, thereby delaying frosting. Experimental results showed that within typical frost-forming temperature ranges (approximately 2-4 C), the heating capacity and COP of the system were significantly improved compared to conventional heat pumps, with reduced power consumption. Additionally, some studies have proposed applying coating treatments to outdoor coil fins to suppress frosting. Li et al.[12]applied superhydrophobic fin-tube heat exchangers in vapor compression heat pumps. Across multiple test conditions, compared to commercial units, the superhydrophobic fin-tube unit achieved a significant reduction in total frost mass (in the range of approximately 59% to 76%) and a concurrent increase in COP (ranging approximately from 11% to 32%). The effectiveness of frost suppression measures through modifying the air parameters at the outdoor coil inlet or hydrophobic treatments on the fins is evident, but due to cost concerns and operational complexity, increasing numbers of researchers have begun focusing on defrosting technologies. Reverse-cycle defrosting remains the most widely used method. However, reverse-cycle defrosting operations involve numerous transient changes in refrigerant, In addition to traditional reverse-cycle defrosting, numerous researchers have proposed novel methods for efficient defrosting of air-source heat pumps. Lyu[17] proposed a defrosting method based on modification and airflow for fin-tube heat exchangers, simulating frosting scenarios. The results showed that this method improved the heat transfer capacity of the heat exchanger by 43.4%. Li [18] proposed a double evaporator air-source heat pump enhanced with injectors temperatures. Other researchers have focused on determining the defrosting start conditions. Chung [14] presented a novel measurement method with frost accumulation amount tracking. This method can monitor the newly - deposited frost amount in real - time, uses the evaporator's volume blockage ratio as the threshold to initiate the defrosting cycle, and has verified the predictive accuracy of the method under different operating conditions. Wang[15] proposed a for defrosting, where the two evaporators alternate during the defrosting process without interrupting heating. The average COP of this system was improved by 20.72% compared to the traditional system. Recently, research on heat storage defrosting has also gained increasing attention. Zhang[19] proposed a method that utilizes waste heat from the compressor shell stored in the heat storage unit for efficient defrosting. Compared to traditional reverse-cycle defrosting, this method reduced defrosting time by 65% and total energy consumption by 27.9%. Qu [20] proposed a heat storage-based cascade air-source heat pump defrosting method, which was compared with conventional hot-gas bypass defrosting. The results showed that the heat storage defrosting method significantly reduced defrosting time and energy consumption, and improved indoor stability. In recent years, increasing numbers of researchers have focused on the defrosting issue of air-source heat pumps. Thanks to the high energy density and narrow temperature fluctuation range of phase change materials[21], they have incomparable advantages in energy storage heating[22], enhanced heating[23], and defrosting[24]. While existing research on ASHP-thermal storage integration focuses on load shifting or defrosting energy supply, a gap exists in strategies enabling concurrent thermal storage preheating and uninterrupted room heating, especially under frosting-prone conditions. Furthermore, comprehensive data on the combined heat storage/release performance and defrosting dynamics of such systems under frosting is scarce.To address these gaps, this study proposes a novel preheating mode within the thermal storage heating mode, using a specific valve configuration (opening the thermal storage inlet valve while closing the outlet valve) for simultaneous storage preheating and room heating. We also systematically evaluate the system's heat storage/release capabilities and defrosting behavior under frosting-prone conditions.

Following the introduction of the experimental setup and working conditions, the paper analyzes the impact of the integrated thermal storage technology and preheating strategy on ASHP system heating performance and defrosting efficiency. Conclusions provide insights for optimizing ASHP-thermal storage systems in challenging frosting environments.

2. Experimental Methods

2.1 Experimental system

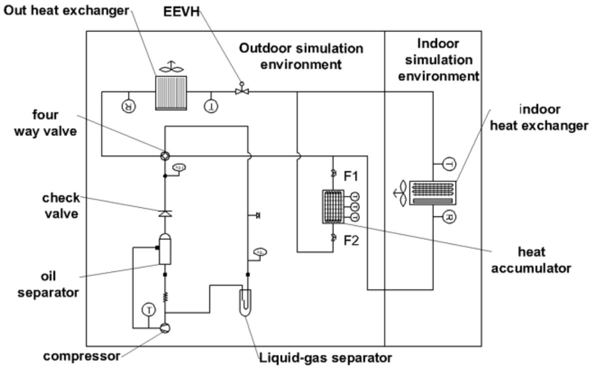

Figure 1. System schematic diagram

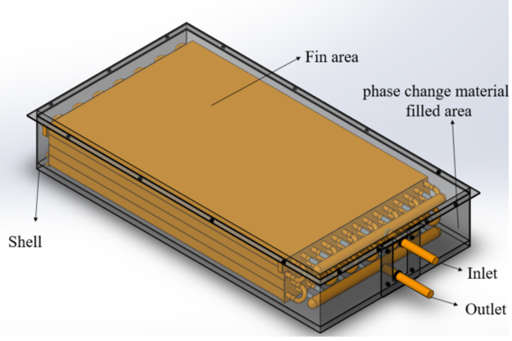

Figure 2. System Structural design of heat accumulator

To better analyze the application of phase-change heat storage coupling in enhancing heating and defrosting for air-source heat pumps (ASHP), a test bench was constructed (as shown in Figure 1), which includes an outdoor environment simulator, an indoor environment simulator, and the ASHP system. The ASHP system consists of a compressor, heat storage unit, outdoor heat exchanger, indoor heat exchanger, four-way reversing valve, solenoid valve, gas-liquid separator, and electronic expansion valve. Using R410a refrigerant, under test conditions of an evaporation temperature of 7.2°C and a condensation temperature of 54.4°C, the system operated for 24 hours with a rated heating capacity of 12.4 kW and a Rated electrical power input is 4.03 kW.

Figure 2 shows the structural design of the heat storage unit, with specific parameters listed in Table 1. In the figure, the yellow area represents the fin region, while the blank space between the shell and copper tubes is the phase change material (PCM) filling area. The refrigerant flows through a main inlet pipe and then splits into seven branches, releasing heat to the PCM while minimizing pressure drop. The outer shell is covered with a 20 mm layer of high-density rubber and plastic insulation.

Table 1. Structural design table for heat accumulator

component	Structural parameters
shell	590*310*80mm
tube	ϕ7*0.5mm
Pipe spacing (longitudinal)	72.76mm
Pipe spacing (transverse)	18.19mm
Fin Size	290*0.2*72.76mm

Table 2 shows the basic parameters of the environmental simulation room, and Table 3 shows the compressor specifications and performance parameters of the heat pump system.

Table 2. Environmental Simulation Range and Accuracy

parameters	Range and Accuracy
Dry bulb temperature on the indoor side	-20~50 ℃，±0.1 ℃
Relative humidity on the indoor side	15~95%，±0.1 ℃
Outdoor Dry Bulb Temperature	-40~60 ℃，±0.1 ℃
Outdoor relative humidity	15~95%，±0.1 ℃
Cooling capacity test range	2.0~15 kW
Heating capacity test range	2.0~16 kW
Measuring range of air volume	4~40 m³/min

Table 3. Compressor Specifications

specification		parameters
compressor	**type**	Piston compressors
	Number of cylinders	2
	exhaust volume cm3	39.2
performances	**cooling capacity W**	12430±5%
	input power W	4030±5%
	Operating current A	14.8
	COP W/W	3.08

In this study, a 5% EG/PA composite phase change material was prepared using the melt blending method. The paraffin-based matrix used is PCM-A-46, with a phase change temperature of 46°C and a latent heat of fusion of 220 kJ/kg. The expanded graphite (EG) has a purity of 99%, a particle size of 75 μ m, and an expansion ratio of 200 times. Table 4 provides the physical properties of the composite phase change material.

Table 4. Physical parameters of 5% EG/PA composite phase change materials

Items	Value	Units
phase transition temperature	46	°C
densities	760	kg/m^3
specific heat capacity	2.1	kJ/(kg·K)
Liquid thermal conductivity	0.2	W/(m·K)
Solid State Thermal Conductivity	0.16	W/(m·K)
latent heat of phase transition	212.41	kJ/kg

2.2 Experimental procedures and conditions

In this study, the heating modes of the heat storage system are illustrated in Figures 3（a）and 3(b), showing the preheating heating mode and the heat storage heating mode, respectively. During the initial operation of the heat pump, indoor heating performance must be prioritized while avoiding excessive power consumption and high compressor speed at startup, thus requiring solenoid valve F2 to remain closed. To prevent an excessively low initial temperature within the heat storage unit, solenoid valve F1 should be opened, allowing a small amount of refrigerant to enter the heat storage unit for preheating. When the average temperature of all sensors in the indoor unit exceeds 30°C, the system switches from preheating mode to heat storage heating mode. The system exits the heat storage mode when the average temperature of all temperature sensors in the heat storage unit reaches or exceeds 50°C during operation. The conventional heating mode involves the compressor discharging refrigerant solely to the indoor unit.

In this study, the defrosting modes of the system are shown in Figures 4(a) and 4(b), which include the conventional defrosting mode and the heat storage defrosting mode. As the frost layer continues to build up, the heat absorption capacity of the evaporator gradually decreases. The system determines whether to enter the defrosting cycle by monitoring the superheat of the refrigerant at the evaporator outlet, with a threshold of 7K. Before entering the defrosting mode, the compressor is first shut down, and after the four-way valve is reversed, the compressor is restarted 30 seconds later. The defrosting mode stops when the temperature of the evaporator outlet pipe reaches the preset value of 22°C.

After the defrost mode ends, the unit's heating capacity becomes insufficient due to the low outdoor coil temperature. Therefore, it is necessary to switch off the indoor fan at this stage and allow the air source heat pump to continue running in heating mode for a period of time, enabling the evaporator temperature to rise and restore normal heating capacity. After the evaporator temperature rises, the indoor fan is turned on again to resume heating. Hence, this energy loss is also considered part of the defrosting loss.

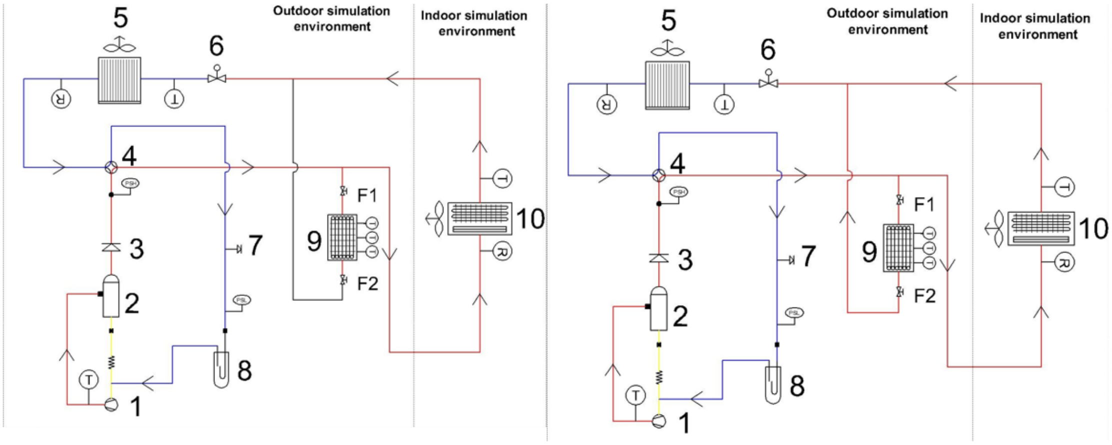

(a) (b)

Figure 3. Preheating heating mode vs. thermal storage heating mode

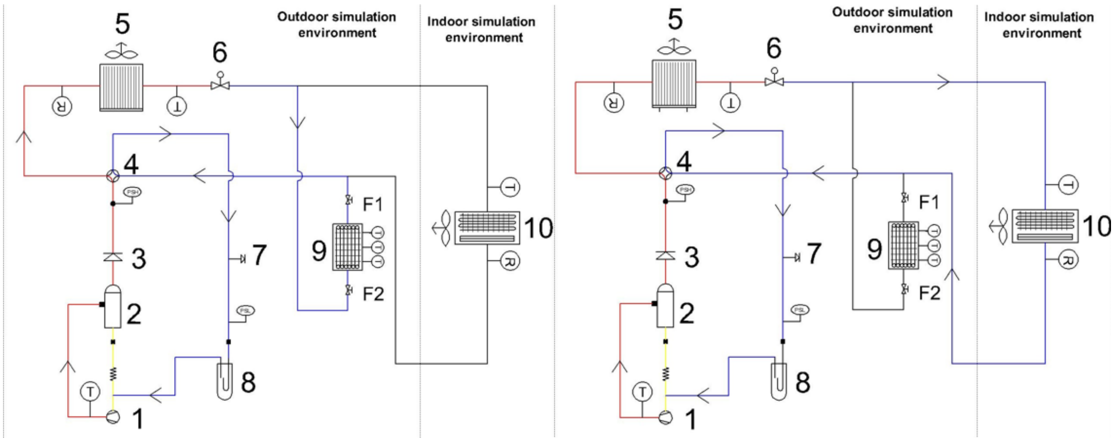

(a) (b)

Figure 4. Thermal storage defrost mode vs. traditional defrost mode

In Figures 3 and 4, the parts are named as follows.1-compressor; 2-oil separator; 3-check valve; 4-four-way reversing valve; 5-outdoor heat exchanger; 6-EEVH; 7-service valve; 8-gas-liquid separator; 9-heat accumulator; 10-indoor heat exchanger

2.3. Data reductions and uncertainty analysis

In this study, the system heating and defrosting performance parameters were evaluated as follows.

The heating capacity of the system and COP is evaluated as[25]:

$$Q_h = C_a m_a \left(T_{a,out} - T_{a,in}\right) \tag{1}$$

$$COP = \frac{\int_0^h Q_h dt}{\int_0^h P dt} \tag{2}$$

where c_a represents the specific heat of air, kJ/(kg·K); m_a represents the mass flow rate of air, kg/s; $T_{a,\ in}$ 、 $T_{a,\ out}$ represent the inlet and outlet temperatures of the indoor unit respectively.

The energy released by the heat accumulator during defrost is evaluated as:

$$Q_{sto} = c_s m\left(t_{sto,int} - t_p\right) + c_l m\left(t_p - t_{sto,end}\right) + mr \tag{3}$$

where c_s and c_l represent the specific heat of the solid and liquid state of the material, kJ/(kg·K); m represents the mass of the material, kg; $t_{sto,\ int}$、 $t_{sto,\ end}$ represent the temperature of the material at the beginning and end of defrosting respectively. Temperature, t_p represents the phase change temperature of the material, °C; r represents the latent heat of phase change of the material, kJ/kg.

The energy released from indoor air during defrost is evaluated as：

$$Q_r = c_a m_a \left(t_{a,int} - t_{a,end}\right) \tag{4}$$

where $t_{a,\ int}$、 $t_{a,\ end}$ respectively represent the indoor air temperature at the beginning and end of defrosting.

The total energy consumption during defrost is evaluated as：

$$Q_{total} = Q_{melt+eva} + Q_{com} \tag{5}$$

$$Q_{melt+eva} = \rho_a v_a \left(w_{a,int} - w_{a,end}\right)\left(L_m + L_e\right) \tag{6}$$

$$Q_{com} = \int_{t,int}^{t,re} P dt \tag{7}$$

where Q_{com} represents the power consumption of the compressor from the beginning of defrost to the end of the heating resume stage; $Q_{melt+eva}$ represents the energy required during defrost and evaporation; $W_{a,int}$, $w_{a,end}$ represent the air volume at the beginning and end of defrost moisture content, g/g; L_m and L_e represent the latent heat of melting and evaporation of water, kJ/kg.

Table 5 shows the table of sensor specifications and accuracy in the experiment. The uncertainty of the experimental data was calculated based on the error propagation equation evaluation as shown in Table 6[26].

Table 5. Sensor specifications and accuracy

measurement parameter	Type	Range ability	Accuracy
Temperature	Pt100	−50°C~ 400°C	±0.1°C
Humidity	HIH-4602	0~100%RH	±3.5%
Power	LT-101A	5~600V/0.002~20A	±0.1%
Pressure	HM200	1-10000000（Pa）	±0.25%

Table 6. Uncertainty of experimental data.

No.	Parameters	Uncertainty
1	System heating capacity	±2.5%
2	COP	±2.8%
3	energy released from the heat accumulator	±1.5%
4	energy released from indoor air	±1.9%
5	Energy from the compressor during resume heating period	±2.2%
6	Energy from defrost and evaporation	±3.3%

3. Results and discussions

3.1. Impact of thermal storage on system heating performance

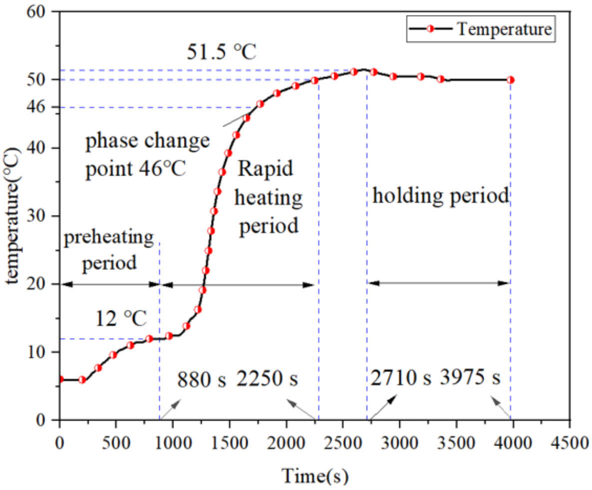

Figure 5. Temperature of phase change material

This section will discuss the impact of the heat storage unit on the system's heating performance. Figure 5 shows the temperature variation of the composite phase change material during the initial startup of the system under outdoor dry/wet bulb conditions of 2/1°C. The initial temperature of the material is 6.5°C, and during the preheating phase, the paraffin temperature increases slowly due to F2 being closed. When the temperature sensors at all indoor unit outlets detect a temperature (R) ≥ 30°C, F2 is opened, the compressor speed increases, and the refrigerant circulation is enhanced, transitioning the heat storage unit into the rapid heat storage mode. During this phase, a high heating rate is maintained until the phase change point of 46°C is reached. After 2250 seconds, the average temperature of the three measurement points in the heat storage unit reaches 50°C, at which point the system exits the heat storage heating mode. Subsequently, due to the thermal inertia of the remaining refrigerant in the pipes and phase change material, the overall average temperature of the material rises to 51.5°C. To verify the insulation performance of the heat storage unit, the system was shut down after completing the heating, and the natural cooling process of the heat storage unit was recorded before 3975 seconds. It can be seen that the heat storage unit exhibits significant insulation performance, with the material temperature remaining in the range of 49±0.5°C.

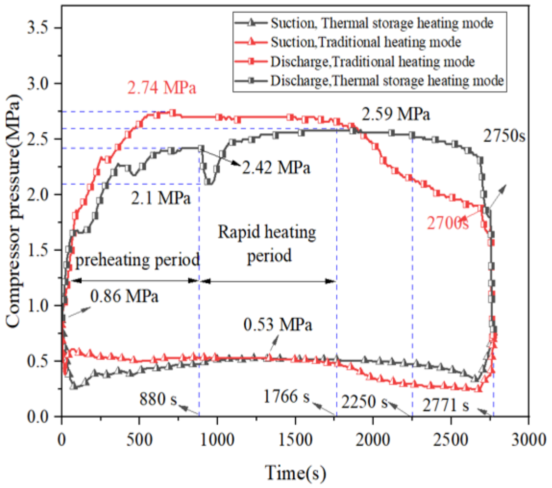

Figure 6 .Suction and discharge pressure of compressor

Figure 6 presents the variations in compressor suction and discharge pressures for both the traditional and heat storage heating modes. In the traditional mode, the discharge pressure gradually increases to 2.74 MPa during the initial operation. After the indoor room temperature reaches the set point, the compressor switches to low-frequency operation, and the discharge pressure slightly decreases, stabilizing at 2.7 MPa. The suction pressure briefly rises before gradually decreasing and stabilizing at 0.53 MPa. After 1766 s, the system experiences increased frosting, causing a decline in discharge pressure, and the defrosting cycle begins at 2700 s. In the heat storage mode, part of the refrigerant is diverted to the heat storage unit, which increases the total condensate, resulting in both suction and discharge pressures being significantly lower than in the traditional mode, with continuous pressure increase. At 880 s, when the system reaches heat storage conditions, the solenoid valve F2 opens, initiating the rapid heat storage phase, and the discharge pressure drops sharply from 2.42 MPa to 2.1

MPa. The rapid heat storage phase continues until 2250 s, when valves F1 and F2 close, and the compressor operates at low frequency. As frosting increases, the refrigerant circulation decreases, causing the discharge pressure to drop, and the system enters the defrosting mode at 2750 s. Overall, during the heat storage phase, the average discharge pressure decreases by 7.3%, and the average suction pressure decreases by 5.1%. Furthermore, due to more effective defrosting in the previous cycle, the frosting time is delayed by 484 s, and the defrosting cycle is postponed by 50 s.

Figure 7 presents the variations in heating capacity and COP between the traditional heating mode and the heat storage heating mode. In the traditional mode, the heating capacity initially increases, reaching a peak of 15702 W with a COP of 2.8. However, after 1766 s, frost accumulation intensifies, resulting in a decline in heating capacity, and the system transitions to the defrosting cycle at 2700 s. In the heat storage mode, the initial trend is similar; however, due to partial refrigerant diversion to the heat storage unit, the heating capacity is slightly lower. At 880 s, when solenoid valve F2 is activated, the heating capacity drops to 13267 W before recovering and stabilizing at 14410 W, with the COP stabilizing at 2.54. After 2250 s, the heat storage unit disconnects, and the heating capacity decreases due to frost formation, with defrosting commencing at 2750 s. Overall, during the heat storage phase, the heating capacity in the heat storage mode is 7.1% lower than that of the traditional mode. However, improved defrosting in the prior cycle delays frost formation, leading to a 1.4% increase in average heating capacity. Nevertheless, as the heat stored in the heat storage unit is solely utilized for defrosting and does not directly contribute to indoor heating, the average COP of the heat storage mode is 5.6% lower than that of the traditional mode.

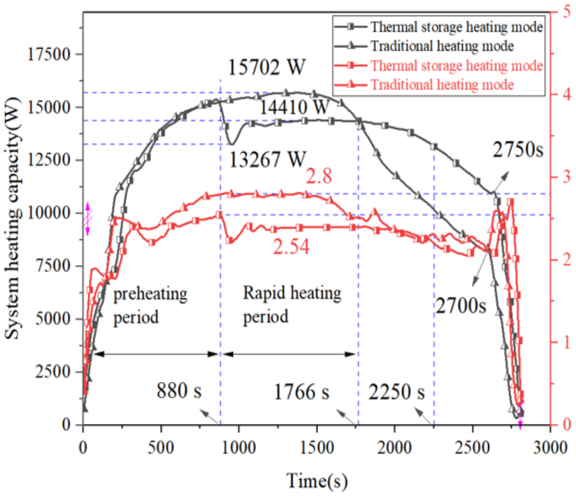

Figure 7. Heating capacity and COP of system

3.2. Impact of thermal storage on system defrost performance

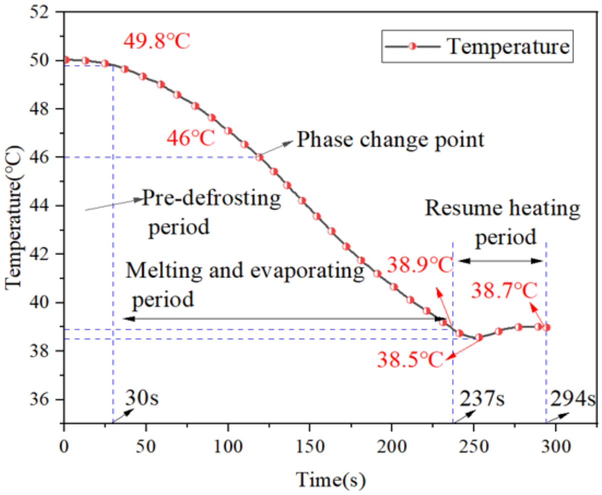

Figure 8. Temperature of phase change material

Figure 8 depicts the temperature variation of the heat storage material during the defrosting process. The initial 30s constitute the pre-frost period, during which the four-way reversing valve completes its reversal. From 30s to 237s marks the melting and evaporating period, during which the heat storage material continuously undergoes exothermic reactions to the refrigerant through the solidification phase change, resulting in a rapid temperature decrease from 49.8°C to 38.9°C. After 237s the system starts to enter the pre-heating mode, a small amount of refrigerant starts to flow into the accumulator, which enters the preheating mode and the temperature starts to recover slowly. As heat has a lag, the overall temperature drops to 38.5°C before it starts to rise.

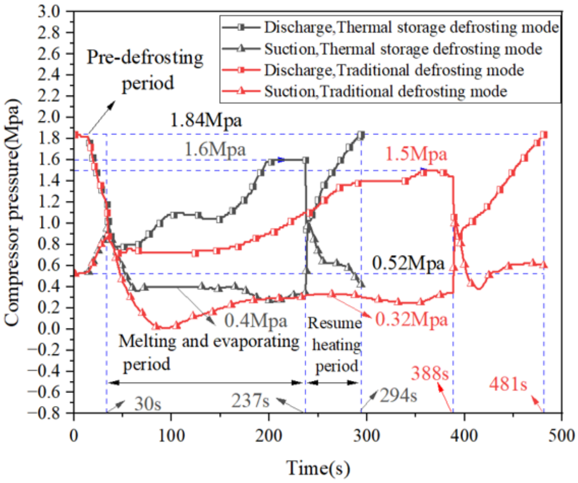

Figure 9. Suction and discharge pressure compressor

Figure 9 illustrates the variations in compressor suction and discharge pressures during the defrosting process for both the traditional and heat storage defrosting modes. At the onset of defrosting, the suction and discharge pressures for both modes are identical, at 0.52 MPa and 1.84 MPa, respectively. During the pre-defrost phase, the compressor is off, and after a 30-second reversal of the four-way valve, the pressures stabilize at approximately 1.0 MPa before the compressor restarts. During the defrost evaporation stage, the discharge pressure rises rapidly, reaching its peak after a brief plateau, while the suction pressure drops to its minimum and then stabilizes. In the heat storage defrosting mode, the discharge pressure peaks at 1.6 MPa, with the suction pressure stabilizing at 0.4 MPa. In contrast, the traditional mode reaches a discharge pressure peak of 1.5 MPa, with the suction pressure stabilizing at 0.32 MPa. The higher temperature of the phase change material in the heat storage unit provides a superior heat source compared to indoor air, resulting in an 18.4% increase in average discharge pressure, a 54.4% increase in average suction pressure, and a 42.2% reduction in defrost evaporation time. After defrosting, the suction and discharge pressures return to atmospheric levels, and the compressor restarts for reheating. During the reheating phase, both modes exhibit similar pressure trends, with the discharge pressure rising to 1.84 MPa, indicating system recovery and readiness for heating. The heat storage defrosting mode achieves reheating in 57 seconds, reducing the recovery time by 38.7% compared to the traditional mode.

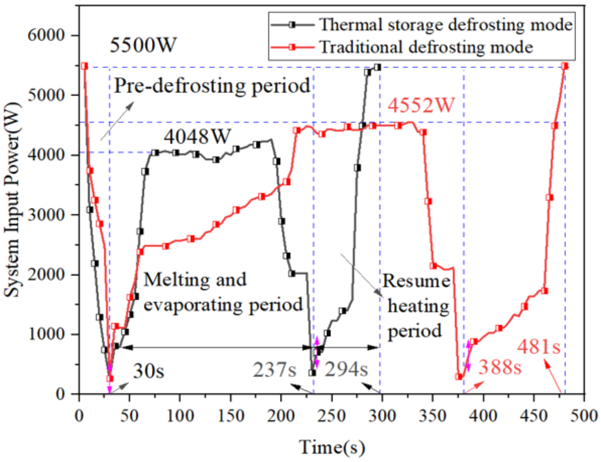

Figure 10. Input power diagram for defrost mode system

Figure 10 illustrates the system input power variations for both the traditional and heat storage defrosting modes. During the pre-defrost phase, the compressor is turned off, and the input power decreases to its lowest point. After the four-way valve reverses, the system enters the defrost evaporation phase, with the compressor operating at 60 Hz. The input power increases, reaching a peak of approximately 4552 W in the traditional mode and completing defrosting in 388 s, while the heat storage mode peaks at around 4048 W and finishes defrosting in 237 s. Following defrosting, the compressor shuts down, and the four-way valve reverses. During the reheating phase, the compressor restarts. Due to the efficiency of the heat storage defrosting mode, the reheating time is reduced to 57 s, compared to 93 s for the traditional mode. Overall, the heat storage defrosting system reduces compressor energy consumption by 480 kJ (42.1%), as shown in Figure 11.

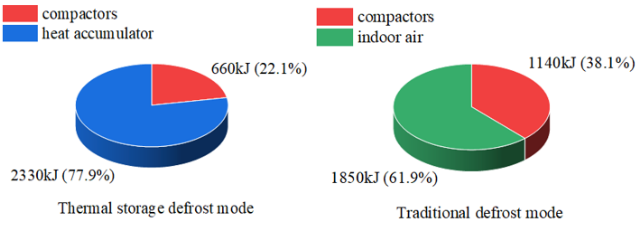

(a) (b)

Figure 11. Energy sources for the two models

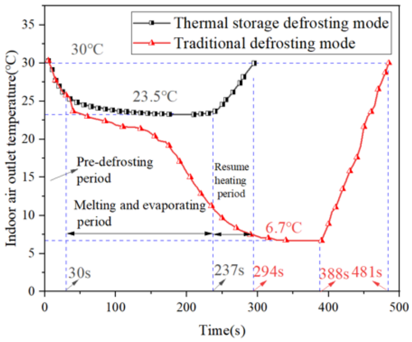

Figure 12. Temperature of indoor outlet air

Figure 12 illustrates the variations in indoor unit outlet air temperature for the traditional and heat storage defrosting modes. During the pre-defrost phase, with the compressor off, the temperatures in both modes decline gradually due to natural heat dissipation from the fan coil, showing similar trends. After 30 seconds, the compressor starts. In the heat storage mode, no

r

e

f

r

i

4. Conclusions

e To combine thermal storage technology with air source heat pumps more efficiently, this study uses 5% EG/PA as thermal storage material to study the heating and defrosting performance of air source heat pump systems based on composite phase change materials. The operating characteristics of the system in heating and defrosting modes were analyzed in detail and the following conclusions were obtained:

1. During the heat storage period of the heat accumulator, the average suction and discharge pressure and heating capacity of the system decreased by 5.1%, 7.3%, and 7.1% respectively. However, from the perspective of the entire heating cycle, more efficient defrosting enables the new system to have a longer heating cycle, in which the frost aggravation time is delayed by 484s and the time to enter the defrost cycle is delayed by 50s, so the overall average heating capacity is increased by 1.4 %, but COP still fell by 5.6%.

f

l

o

w

s

i

2. The compressor suction and discharge pressures in the thermal storage defrost cycle are increased by 54.4% and 18.4%, respectively, compared with the traditional defrost mode. At the same time, the defrost time is shortened, specifically, the defrost evaporation period is reduced by 42.2%, and the heating resume period is reduced by 38.7%, and the power consumption of the compressor is reduced by 480 kJ, which is 42.1% lower than the traditional defrost system.

n

t

o

t

h

3. Compared with the traditional defrosting system, the temperature fluctuation at the outlet

e o

f

i

n t

d h

o e

In summary, the main value proposition of a thermal storage system is the ability to maintain a stable outlet temperature during defrost, thereby significantly improving indoor temperature fluctuations and addressing the major drawbacks of conventional systems. However, these benefits come at the cost of lowering the overall system COP as well as increasing system complexity, space requirements, and initial investment. Future efforts should focus on optimizing PCM selection, TES equipment design, and system controls to minimize efficiency losses and cost impacts.

Acknowledgement

This work was supported by the Royal Society of Chemistry Research Fund (Grant No. R23-8089911052).

Nomenclature

C	– Specific heat capacity, [J kg^{-1} K^{-1}]	t_{sto}, int	– Temperature of the material at the beginning of defrost, [°C]
K	– Thermal conductivity, [W m^{-1} K^{-1}]	ρ_a	– Density of air, [kg/m^3]
Re	– Reynolds number, [–] (Equation: Re = UD / ν)	t_a, int	–Indoor air temperature at the beginning of defrost, [°C]
C_a	– Specific heat of air, [kJ/(kg·K)]	t_a, end	– Indoor air temperature at the end of defrost, [°C]
c_s	– Specific heat of the solid state of the material, [kJ/(kg·K)]	W_a	– air moisture content,[g/g]
c_l	– Specific heat of the liquid state of the material, [kJ/(kg·K)]	Greek Symbols	
L_e	– Latent heat of evaporation of water, [kJ/kg]	α	– Thermal diffusivity, [m^2 s^{-1}]
L_m	– Latent heat of melting of water, [kJ/kg]	β	–Thermal expansion coefficient, [K^{-1}]
m_a	– Mass flow rate of air, [kg/s]	μ	– Dynamic viscosity, [Pa·s]
Q_{sto}	– Energy released by the heat accumulator during defrost, [kJ]	ρ	– Density, [kg m^{-3}]
Q_r	– Energy released from indoor air during defrost, [kJ]	σ	– Stefan-Boltzmann constant, [W m^{-2} K^{-4}]
T	– Temperature, [K]	Acronym	
T_a, in	– Inlet temperature of indoor air, [°C]	COP	– Coefficient of Performance
T_a, out	– Outlet temperature of indoor air, [°C]		

References

[1] HAO F, SHAO W. What really drives the deployment of renewable energy? A global assessment of 118 countries[J/OL]. Energy Research & Social Science, 72(2021), 101880. DOI:10.1016/j.erss.2020.101880.

[2] ZHAO X, LUO D. Driving force of rising renewable energy in China: Environment, regulation and employment[J/OL]. Renewable and Sustainable Energy Reviews, 68(2017), pp. 48-56. DOI:10.1016/j.rser.2016.09.126.

[3] ZHANG L, JIANG Y, DONG J, et al. . Advances in vapor compression air source heat pump system in cold regions: A review[J/OL]. Renewable and Sustainable Energy Reviews, 81

(2018), pp. 353-365. DOI:10.1016/j.rser.2017.08.009.

[4] SONG M, DENG S, DANG C, et al. . Review on improvement for air source heat pump units during frosting and defrosting[J/OL]. Applied Energy, 211(2018), pp. 1150-1170. DOI:10.1016/j.apenergy.2017.12.022.

[5] RUAN F, QIN D, XU S, et al. . Study on the optimization of heat loss during operation of air source heat pump based on entransy theory[J/OL]. Thermal science, 28(2024), 4, pp. 3039-3048. DOI:10.2298/TSCI231016078R.

[6] SHEN J, GUO T, TIAN Y, et al. . Design and experimental study of an air source heat pump for drying with dual modes of single stage and cascade cycle[J/OL]. Applied Thermal Engineering, 129(2018), pp. 280-289. DOI:10.1016/j.applthermaleng.2017.10.047.

[7] LIU G, XIONG T, SUN T, et al. . Frosting and defrosting characteristics of household refrigerators and freezers: Recent progress and perspectives[J/OL]. Energy and Buildings, 303(2024), 113755. DOI:10.1016/j.enbuild.2023.113755.

[8] WEI W, FENG Z, NI L, et al. . Frosting suppression performance enhancement of air source heat pump through improving relative capacity[J/OL]. Applied Thermal Engineering, 236(2024), 121698. DOI:10.1016/j.applthermaleng.2023.121698.

[9] WU C, LIU F, LI X, et al. . Low-temperature air source heat pump system for heating in severely cold area: Long-term applicability evaluation[J/OL]. Building and Environment, 208(2022), 108594. DOI:10.1016/j.buildenv.2021.108594.

[10] SU W, LI W, ZHANG X. Simulation analysis of a novel no-frost air-source heat pump with integrated liquid desiccant dehumidification and compression-assisted regeneration[J/OL]. Energy Conversion and Management, 148(2017), pp. 1157-1169. DOI:10.1016/j.enconman.2017.06.059.

[11] KWAK K, BAI C. A study on the performance enhancement of heat pump using electric heater under the frosting condition: Heat pump under frosting condition[J/OL]. Applied Thermal Engineering, 30(2010), 6, pp. 539-543. DOI:10.1016/j.applthermaleng.2009.10.016.

[12] LI R, WANG Z, ZHANG Y, et al. . Performance improvement of vapor compression heat pump with superhydrophobic finned-tube evaporator[J/OL]. Journal of Building Engineering, 87(2024), 109013. DOI:10.1016/j.jobe.2024.109013.

[13] QU M, LU M, LI Z, et al. . Thermal energy storage based (TES-based) reverse cycle defrosting control strategy optimization for a cascade air source heat pump[J/OL]. Energy and Buildings, 219（2020）, 110014. DOI:10.1016/j.enbuild.2020.110014.

[14] CHUNG Y, NA S I, YOO J W, et al. . A determination method of defrosting start time with frost accumulation amount tracking in air source heat pump systems[J/OL]. Applied Thermal Engineering, 184(2021), 116405. DOI:10.1016/j.applthermaleng.2020.116405.

[15] WANG W, ZHOU Q, TIAN G, et al. . A novel defrosting initiation strategy based on convolutional neural network for air-source heat pump[J/OL]. International Journal of Refrigeration, 128(2021), pp. 95-103. DOI:10.1016/j.ijrefrig.2021.04.001.

[16] MA L, WANG F, WANG Z, et al. . Experimental investigation on an air source heat pump system with coupled liquid-storage gas-liquid separator regarding heating and defrosting performance[J/OL]. International Journal of Refrigeration, 134(2022), pp. 176-188. DOI:10.1016/j.ijrefrig.2021.11.025.

[17] LYU N, SHAO Z, HE H, et al. . Performance study of an active-passive combined anti-frosting method for fin-tube heat exchanger[J/OL]. Building and Environment, 222　3(2022),

109365. DOI:10.1016/j.buildenv.2022.109365.

[18] LI S, LU J, LI W, et al. . Thermodynamic analyses of a novel ejector enhanced dual-temperature air source heat pump cycle with self-defrosting[J/OL]. Applied Thermal Engineering, 215(2022), 118944. DOI:10.1016/j.applthermaleng.2022.118944.

[19] LIU Z, ZHAO F, ZHANG L, et al. . Performance of bypass cycle defrosting system using compressor casing thermal storage for air-cooled household refrigerators[J/OL]. Applied Thermal Engineering, 130(2018), pp. 1215-1223. DOI:10.1016/j.applthermaleng.2017.11.077.

[20] QU M, LI T, DENG S, et al. . Improving defrosting performance of cascade air source heat pump using thermal energy storage based reverse cycle defrosting method[J/OL]. Applied Thermal Engineering, 121(2017), pp. 728-736. DOI:10.1016/j.applthermaleng.2017.04.146.

[21] CHEN X. Analysis of thermal characteristics and thermal storage performance of energy-saving phase change thermal storage materials in buildings[J/OL]. Thermal science, 28(2024), 2B, pp. 1509-1517. DOI:10.2298/TSCI2402509C.

[22] SHI L, HUANG C, ZHENG N, et al. . Thermal energy storage characteristics of carbon-based phase change composites for photo-thermal conversion[J/OL]. Journal of Energy Storage, 77(2024), 109892. DOI:10.1016/j.est.2023.109892.

[23] BHARATHIRAJA R, RAMKUMAR T, SELVAKUMAR M. Studies on the thermal characteristics of nano-enhanced paraffin wax phase change material (PCM) for thermal storage applications[J/OL]. Journal of Energy Storage, 73(2023), 109216. DOI:10.1016/j.est.2023.109216.

[24] LI Z L, ZHANG C L, LIU H M, et al. . Feasibility analysis of thermal storage defrosting method for air source heat pump: From energetic and economic viewpoints[J/OL]. Applied Thermal Engineering, 236(2024), 121828. DOI:10.1016/j.applthermaleng.2023.121828.

[25] XU Z, HAN L. An experimental study on energy-storage based defrosting performance of an air source heat pump system with a micro-channel heat exchanger as outdoor coil[J/OL]. Applied Thermal Engineering, 240(2024), 122067. DOI:10.1016/j.applthermaleng.2023.122067.

RECEIVED DATE: 17.3.2025.
DATE OF CORRECTED PAPER: 22.4.2025.
DATE OF ACCEPTED PAPER: 16.7.2025.